HHS Public Access

Author manuscript

Environ Pollut. Author manuscript; available in PMC 2024 October 01.

Published in final edited form as:

Environ Pollut. 2023 October 01; 334: 122183. doi:10.1016/j.envpol.2023.122183.

Environmentally Persistent Free Radicals: Methods for combustion generation, whole-body inhalation and assessing cardiopulmonary consequences

Ankit Aryal[1], **Alexandra Noël**[1], **Lavrent Khachatryan**[2], **Stephania A. Cormier**[3], **Pratiti H. Chowdhury**[3], **Arthur Penn**[1], **Tammy R. Dugas**[1,*], **Ashlyn C. Harmon**[1,*,#]

[1]Department of Comparative Biomedical Sciences, Louisiana State University School of Veterinary Medicine, Baton Rouge, Louisiana 70803.

[2]Department of Chemistry, Louisiana State University A&M College, Baton Rouge, Louisiana 70803

[3]Department of Biological Sciences, Louisiana State University A&M College and the Pennington Biomedical Research Institute, Baton Rouge, Louisiana 70803.

Abstract

Particulate matter (PM) containing environmentally persistent free radicals (EPFRs) results from the incomplete combustion of organic wastes which chemisorb to transition metals. This process generates a particle-pollutant complex that continuously redox cycles to produce reactive oxygen species. EPFRs are well characterized, but their cardiopulmonary effects remain unknown. This publication provides a detailed approach to evaluating these effects and demonstrates the impact that EPFRs have on the lungs and vasculature. Combustion-derived EPFRs were generated (EPFR lo: $2.1e^{-16}$ radical/g, EPFR hi: $5.5e^{-17}$ radical/g), characterized, and verified as representative of those found in urban areas. Dry particle aerosolization and whole-body inhalation were established for rodent exposures. To verify that these particles and exposures recapitulate findings relevant to known PM-induced cardiopulmonary effects, male C57BL6 mice were exposed to filtered air, ~280 μg/m^3 EPFR lo or EPFR hi for 4 hr/d for 5 consecutive days. Compared to filtered air, pulmonary resistance was increased in mice exposed to EPFR hi. Mice exposed to EPFR hi also exhibited increased plasma endothelin-1 (44.6 vs 30.6 pg/mL) and reduced nitric oxide (137 nM vs 236 nM), suggesting vascular dysfunction. Assessment of vascular response demonstrated an

[#]Address all correspondence to: ashlynharmon@lsu.edu.
[*]Authors contributed equally to this manuscript.

AUTHOR STATEMENT

Ankit Aryal: Investigation, Writing-Original Draft, Formal Analysis; **Alexandra Noël:** Investigation, Conceptualization, Writing-Review and Editing; **Lavrent Khachatryan:** Investigation; Writing-Original Draft **Stephania A. Cormier:** Funding Acquisition, Conceptualization; **Pratiti H. Chowdhury:** Investigation; **Arthur Penn:** Resources; **Tammy R. Dugas:** Funding Acquisition, Conceptualization, Writing-Review and Editing, Supervision; **Ashlyn C. Harmon:** Project Administration, Conceptualization, Writing-Review and Editing, Supervision.

Declaration of interests

The authors declare that they have no known competing financial interests or personal relationships that could have appeared to influence the work reported in this paper.

impairment in endothelium-dependent vasorelaxation, with maximum relaxation decreased from 80% to 62% in filtered air vs EPFR hi exposed mice. Gene expression analysis highlighted fold changes in aryl hydrocarbon receptor (AhR) and antioxidant response genes including increases in lung *Cyp1a1* (8.7 fold), *Cyp1b1* (9 fold), *Aldh3a1* (1.7 fold) and *Nqo1* (2.4 fold) and *Gclc* (1.3 fold), and in aortic *Cyp1a1* (5.3 fold) in mice exposed to EPFR hi vs filtered air. We then determined that lung AT2 cells were the predominate locus for AhR activation. Together, these data suggest the lung and vasculature as particular targets for the health impacts of EPFRs and demonstrate the importance of additional studies investigating the cardiopulmonary effects of EPFRs.

Graphical Abstract

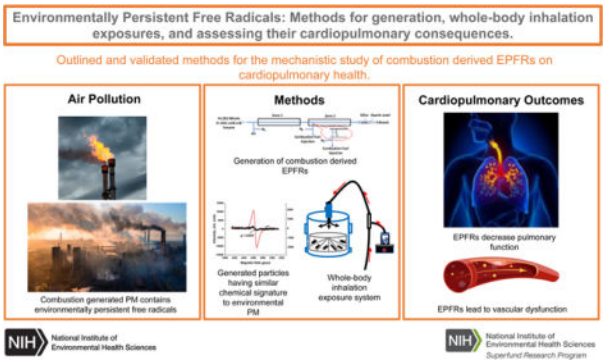

Keywords

Environmentally Persistent Free Radicals; Cardiovascular Health; Particulate Matter; Cardiopulmonary; Environmental Toxicology; Inhalation

1. Introduction

Thermal remediation of organic waste is commonly employed at abandoned hazardous wastes facilities that fall under the US Comprehensive Environmental Response, Compensation, and Liability Act of 1980 (Davis, 2020; Svatos, 2022). However, thermal remediation is an accepted method of hazardous waste reduction in countries around the globe, even though its health impacts are not yet fully elucidated. A primary health concern associated with burning organic wastes is the inhalation of fine (diameter < 2.5 μm) and ultrafine (diameter < 0.1 μm) particulate matter produced during combustion processes (Rajagopalan et al., 2020). Particulate matter (PM) is the complex mixture of solid particles and liquid droplets suspended in air, with sources ranging from dust and dirt to smoke and soot (Pope 3rd, 2000).

PM air pollution affects the respiratory system directly; however, epidemiological studies have consistently demonstrated a strong correlation between increased combustion-generated PM levels and both pulmonary and cardiovascular events (Aryal et al., 2021). The Global Burden of Diseases, Injuries and Risk Factors study of 2015 estimated that ambient $PM_{2.5}$ air pollution is the fifth highest risk factor for mortality (Cohen et al.,

2017). Deaths attributed to $PM_{2.5}$ is estimated at 4.2 million, representing 7.6% of total global mortality (Cohen et al., 2017), and increases in PM concentrations correlate with the development of chronic obstructive pulmonary disease (COPD), asthma, and reduced pulmonary function. Some studies showed that even short-term exposure at levels at or below the US National Ambient Air Quality Standards is associated with lower lung function (Mary et al., 2013; Rice et al., 2013). Moreover, the European Study of Cohorts for Air Pollution Effects (ESCAPE) project, a prospective study and meta-analysis of 11 European cohorts, showed an association between long-term PM exposure and an increased incidence of coronary events, and this association persisted even at the exposure levels below European standard limit values (Cesaroni et al., 2014). ESCAPE also demonstrated that an annual 5 $\mu g/m^3$ increase in $PM_{2.5}$ levels increased risks of coronary events by 13%, and a 10 $\mu g/m^3$ annual increase of PM_{10} increase the risk of coronary events (Cesaroni et al., 2014). Additionally, PM air pollution is linked with increased hospitalization admissions associated with pulmonary (Çapraz & Deniz, 2021; Xie et al., 2019; Yang et al., 2021) and cardiovascular-related diseases (Le et al., 2014; Motesaddi Zarandi et al., 2022; Wyatt et al., 2022; Wyatt et al., 2020).

PM formed during the thermal remediation of organic waste and contaminated soils contains free radicals. Our colleagues and researchers worldwide have identified these free radicals, termed Environmentally Persistent Free Radicals (EPFRs), as a new class of emerging pollutants (Dela Cruz et al., 2014; Dellinger et al., 2000; Dellinger et al., 2001; Filippi et al., 2022; Gehling et al., 2014; Li et al., 2023; Lomnicki & Dellinger, 2003; Lomnicki et al., 2008; Runberg et al., 2020; Wang et al., 2019; Xu et al., 2021). During the thermal treatment of organics wastes, incomplete combustion of hydrocarbons occurs due to oxygen-poor pockets within and on the outer edges of the flame. These combustion products chemisorb to transition metal oxides within the particle, producing a free radical complex. These complexes often contain surface stabilized semiquinone- and phenoxy-type radicals that behave as a unique particle-pollutant system (i.e., as EPFRs). The importance of EPFRs is emerging worldwide (Alaghmand & Blough, 2007; DiStefano et al., 2009; Fang et al., 2014; Pan et al., 2004; Tian et al., 2009). These free radicals are weakly reactive with the oxygen species, conferring their ability to persist in the ambient air from a few hours to several months. Studies have shown that EPFRs can generate reactive oxygen species such as hydroxyl and superoxide radicals, and consequently, are able to induce oxidative stress in biological systems. Moreover, this pollutant-particle system often confers a more significant toxicity than its individual constituents alone (Kelley et al., 2013; Zhang et al., 2020). It should be noted that similar semi-quinoid radicals are associated with particulate matter generated from cigarette smoke (Pryor et al., 1998) and other combustion sources (Valavanidis et al., 2006). Furthermore, several studies demonstrating semiquinone radicals have been found in PM collected from urban areas (Dellinger et al., 2001; Lingard et al., 2005; Valavanidis et al., 2005; Valavanidis et al., 2008). Approximately 78 million Americans, accounting for 24% of the U.S. population, reside within 3 miles of Superfund sites where significant PM-containing EPFRs have been detected (Dela Cruz et al., 2014; Oyana et al., 2017). Thus, studies examining the biological mechanisms by which these free radicals elicit toxicity, including both exposure and risk assessment analyses, are critical for ensuring public health and safety.

In the last 20 years, environmental research related to EPFR generation and airborne exposures has increased dramatically, with PubMed indexed reports increasing nearly 300-fold between the years 2006 and 2022. Despite this, there is limited literature documenting the human health effects of EPFRs, owing in part to a lack of relevant animal models and exposure techniques. Studies aimed at elucidating the cardiopulmonary impacts of EPFRs are even less documented and rectifying this void is imperative for devising risk mitigation strategies and protective interventions. The primary objective of this study was to provide a validated, methodological approach for conducting EPFR toxicology studies in rodent species in a manner that closely mimics airborne exposure and EPFR inhalation. These studies also established and validated new methods for the laboratory generation of combustion-derived EPFRs, for dry particle aerosolization, and for whole body inhalation exposures of mice. Our ultimate goal was to make these methods accessible and achievable by other investigators in the field of cardiovascular and cardiopulmonary toxicology, so that collectively, we can begin to address the health impacts of EPFRs. We also provide a detailed description of our exposure setup and the parameters used to achieve experimental conditions that are relevant to human exposure scenarios. Finally, we include measures of cardiopulmonary function and expression profiling to identify whether our EPFR inhalation paradigm elicits health effects in rodents and to characterize the signal transduction mechanisms that may be involved.

2. Methods

EPFR preparation

EPFRs were synthesized through the catalytic combustion of 1-methyl naphthalene in presence of anthracene and an additive, monochlorophenol. Note that monochlorophenol was used as a chlorinated organic compound representative of chlorinated organics typically found in Superfund sites in Louisiana, particularly those originating from wood treatment facilities. A new Two Stage Combustion Reactor (TSCR; Figure 1A) was developed to generate EPFRs with a well-defined and controlled radical composition. Specifically, this reactor provides an accurate control over EPFR concentration, but also allows for the addition of other organic pollutants and metals of environmental concern.

The design of the TSCR reactor is based on our published studies to investigate the sooting phenomenon of 1-methylnaphtalene in the gas phase (Herring et al., 2015; M. P. Herring et al., 2013; P. Herring et al., 2013). Briefly, Zone 1 of the dual zone reactor generates entrained metal oxide nanoparticles from the high-temperature oxidation of reverse micelle suspension of metal oleate in hexane. The Zone 1 reactor is maintained at 700°C with a gas-phase residence time of 60 seconds. It interfaces with the Zone 2 combustor, where gases containing particles from Zone 1 are transported in a gas phase passing through a cooling section to ensure nucleation of the metal oxide nanoparticles before reaching Zone 2.

Oxidative pyrolysis occurring in the Zone 2 combustor operates at sub-stoichiometric combustion conditions typical for oxygen-starved pockets in thermal treatment systems (Walsh et al., 2010). The Zone 2 reactor is maintained at 975˚C with a gas-phase residence time of 1 second. The flow rate of the carrier gas (54 cc/min) ensures the introduction of

fuel to the Zone 2 reactor by syringe pump, with no back flow of the gases into Zone 1. The combustion fuel is delivered into Zone 2 through a side port arm (Figure 1A). The control of EPFR concentration is achieved by changing the parametric combustion conditions, specifically, by adjusting the cross-sectional location of the fuel injection point in Zone 2. Figure 1A also presents the cross-sectional temperature gradient in the fuel injection area and injection locations. We are typically able to produce particles with two different characteristics we term EPFR hi, or particles containing of ~1×10^{18} spins/g (i.e., free radicals/g), and EPFR lo, containing 1×10^{16} spins/g.

To initiate EPFR synthesis, suspensions of the metal ion–oleate micelles are prepared using a metal nitrate (typically Fe) with oleic acid in hexane. The mixture is vigorously stirred until the ferric ion is transferred into the oleic acid layer, producing a dark red color. Then the upper layer is collected and further diluted in hexane to reach the desired metal concentration. We used 0.02 M solution of $Fe(NO_3)_3$ in hexane for these studies. The micelles are then introduced through a septum into Zone 1 using a syringe pump maintained at 85 μL/h. The concentration of metal introduced into Zone 1 is adjusted to achieve metal concentrations in the final EPFR-containing PM in the range of 1–50 ppm.

The EPFRs generated in the TSCR are collected thermophoretically onto a Cab-o-Sil fumed silica matrix contained at the exit of Zone 2 (Figure 1A). Cab-o-Sil is a solid powder with a particle diameter <0.2 μm. The collection of PM on Cab-o-Sil is based on the adhesion of effluent EPFR to the matrix particles. The collection matrix is easily transferable to any media and disperses in water and other solvents with shaking or short sonication. This ensures quantitative transfer of collected samples, eliminating labor intensive and inefficient particle recovery.

To avoid secondary effects of large amounts of polycyclic aromatic hydrocarbons (PAHs) (Morgan et al., 2008) that may interfere with our ability to tease apart the health impacts of EPFRs, *per se*, the particles are subjected to vacuum drying at 50°C for 45 minutes, which essentially removes most of the physiosorbed PAHs while the concentration of EPFRs remains unchanged. Pilot experiments demonstrated that sample yields from TSCR are dependent on fuel-to-air equivalence ratio, the temperature in Zone 2, and the concentration of the introduced metal. Approximately 10 mg of sample is generated (Supplemental Figure 1) in a 45 min experiment, where Zone 2 is maintained at 975°C, with an Fe(II) oxide content ~10 ppm in the gas phase and where the fuel-to-air ratio is sustained at 2.5, indicating an oxidative pyrolysis condition (M. P. Herring et al., 2013). Typical EPR spectra for EPFR hi and low particles generated using the TSCR are characterized by a relatively broad (ΔHp-p ~6 –10 Gauss), asymmetric signal with g value of 2.0028–2.0036 (Figure 2A).

EPFR characterization and half-life

The EPR spectra obtained from EPFR hi and lo particles generated using the TSCR system typically exhibit an asymmetric signal with a g value of 2.0028–2.0032 and a relatively broad (ΔHp-p ~6 –10 Gauss) peak, as shown in Figure 2A. EPFRs have a defined lifetime, which is the time (t) taken for their initial concentration to decrease by a factor of 1/e (where **e** is the natural logarithm base). The lifetime of EPFRs in pseudo-1st order decay reactions

can be expressed as $t_{1/e} = 1/k$, where k is the rate constant for the decay reaction of EPFRs and can be determined experimentally using the standard equation:

$$\log C/Co = -(k/2.3) \times t \quad \text{(Equation 1)}$$

In equation 1, Co and C represent the initial and current concentration of EPFRs, respectively, and k is the rate coefficient for the pseudo-unimolecular decay reaction of EPFRs. EPR is used to measure the intensity of the radical signal. To perform the EPR measurement, 10–15 mg particulate is transferred and sealed into an EPR tube, and the measurement is taken promptly to track any changes (i.e., aging) of the radicals over time.

The concentration of EPFRs (number of spins, Co or C) was determined using the following equation (Eaton et al., 2010):

$$C(\text{ or } Co) = [(DI/N)\text{ sample }/(DI/N)\text{ standard }] \times C\text{ standard} \quad \text{(Equation 2)}$$

Here, the DI/N ratio represents the normalized double integration of the EPR spectrum for both the sample and standard. A DPPH solid sample with a known spin content was used as the EPR standard. To ensure a similar magnetic field distribution, a 5 mm EPR tube was used for both the sample and standard, maintaining the same quality value (Q value) of the EPR resonator. The WINEPR software automatically calculated the DI/N ratio by considering the receiver gain, time constant, and sweep time for the radicals, among other factors (Eaton et al., 2010). The final concentration of radicals in spins/g was obtained by dividing the number of spins calculated using formula (2) by the sample mass in grams.

EPFR hi containing particles were aged from June 30 to September 9, 2020. The exponential fit is represented by a red dashed line with an equation $Y = 2.0*10^{17}\exp(-0.0002*t)$, where Y is EPFR concentration in spins/g, and t is aging time in hours. As described in equation 1, the $t_{1/e}$ is determined as 1/0.0002, which equals 5000 hours, approximately equivalent to 208 days. It is important to note that the half-life of the radicals, denoted as $t_{½}$ (the time taken for the initial concentration to decrease by half), is related to the 1/e time ($t_{1/e}$) by the formula $t_{½} = \ln 2/k = \ln 2*(t_{1/e})$. Consequently, the half-life of EPFRs is calculated as 0.63 multiplied by 208, resulting in 131 days.

Dry particle aerosolization and whole-body inhalation

All animal procedures were approved in advance by the LSU Institutional Animal Care and Use Committee and adhered to the principles established in the *Guide for the Care and Use of Laboratory Animals* (8th ed). Male C57BL/6 mice were obtained at 17–19 wk of age from Jackson Laboratory (Bar Harbor, ME). Mice were acclimated to the room for 1 wk, maintained on a regular 12-h light/12-h dark cycle and allowed *ad libitum* access to food and water. At 18–20 wk of age, the mice were exposed to filtered air or to 280±49.9 μg/m^3 EPFR hi, or 278±47.4 μg/m^3 EPFR lo, for 4 hours. As such, particle mass concentrations remained similar while the free radical concentration varied between treatment groups. The mice were then returned to their cages and the exposures were continued at 4 hours/day for 5 days. It should be noted that based upon our prior studies of airborne PM, the

EPFR concentrations compared here (1×10^{16} for EPFR lo versus 1×10^{18} radicals/g for EPFR hi) are environmentally relevant. For example, assessments of EPFR concentrations in Memphis, TN demonstrated that airborne PM contains $1.1e^{17}$–$3.7e^{19}$ radicals/g (Oyana et al., 2017). Assuming the NAAQS 24 h compliance concentration for $PM_{2.5}$ of 35 μg/m^3 and measured EPFR concentrations of $1.1e^{17}$–$3.7e^{19}$ radicals/g, EPFR/m^3 concentrations in Memphis would be estimated at $3.9e^{12}$–$1.3e^{15}$ EPFR/m^3. Studies conducted here exposed mice at $2.8e^{12}$–$2.4e^{14}$ EPFR/m^3 (assuming 1×10^{16}-1×10^{18} EPFR/g × 280×10^{-6} g/m^3).

We used a whole-body inhalation system described in Harmon et al (Harmon et al., 2021). For inhalation exposures, C57BL/6 male mice were placed in an 18-L Plexiglas chamber containing 16 individual compartments (Figure 1B). Animals were thus separated from one another during exposures, prohibiting their ability to cuddle or lick one another. It also allowed for simultaneous exposure of multiple mice at a single EPFR concentration. Male mice were chosen for this methods development study because prior studies showed males are more susceptible than females to the effects of ultrafine PM inhalation (Noël et al., 2017; Woodward et al., 2019; Xiao et al., 2013). Mice were exposed to filtered air (controls) compared to a consistent 280±47.4 μg/m^3 EPFR hi or 278±49.9 μg/m^3 EPFR lo aerosols generated *via* a dry dispersion technique (Figure 1C) (Harmon et al., 2021). Using a Venturi disperser (Noël et al., 2012), 25–27 mg EPFR particles were aerosolized by adjusting HEPA-filtered airflow maintained ~7 L/min to achieve the desired EPFR concentrations. Prior studies by our team (Harmon et al., 2021) established the uniformity of particle distribution within the chamber, where we typically achieve ±20% of the targeted mass concentration. Moreover, exhaust flow (1–2 L/min) at the bottom of the chamber removed aerosolized particles and allowed for air exchanges. A TSI DustTrak II Model 8530 (Shoreview, MN) was used to measure total mass concentration in the chamber at 1 second intervals. Precise determination of total mass concentration was measured gravimetrically by applying a glass fiber filter across an exhaust stream, to which a Sensidyne Gilian BDX-II air sampling pump (Sensidyne, St-Petersburg, FL) was applied. Additionally, aerosolized particle characterization was assessed by electron microscopy and directly by using a scanning mobility particle sizer spectrometer (SMPS) (TSI, Inc., Shoreview, MN). After each 4-hour exposure, exposed animals were returned to their cages where they breathed HEPA-filtered air. Immediately after the last 4-hour exposure, pulmonary function was measured in the mice under sedation, after which they were euthanized by injection of Beuthanasia-D intraperitoneally. Eight mice from each group were used for pulmonary function measures, lung histopathology and gene expression in the lung. The remaining eight mice in each group were used for evaluation of vascular reactivity, plasma biomarkers of endothelial function and gene expression in excised aortas, representative of a vascular tissue peripheral to the lung.

Characterization of EPFR aerosols

Aerosolized EPFR particles were characterized for morphology, agglomerate structure, and size by transmission electron microscopy (TEM). As previously described (Harmon et al., 2021; Noël et al., 2013), during EPFR particle exposure, samples of aerosolized EPFR particles were collected using a cassette containing a polycarbonate filter onto which a precoated carbon Formvar copper grid was glued. Samples were collected for 5 minutes at

a flow rate of 1 L/min. Visualization of the aerosolized particles was conducted using a JEOL JEM-1010 TEM microscope. Additionally, we used a scanning mobility particle sizer spectrometer (SMPS) (Model 3938L50, TSI Inc., Shoreview, MN) to determine the particle size distribution of aerosols composed of EPFR lo or EPFR hi particles. This particle sizing system is composed of a classifier (Model 3082), a long differential mobility analyzer (DMA) (Model 3081A), and a condensation particle counter (CPC) (Model 3750), all from TSI Inc. (Shoreview, MN). This system is also equipped with an aerosol neutralizer (Kr-85, 370 MBq/10 mCi) (Model 3077A, TSI Inc., Shoreview, MN). The operating principal of the SMPS is particle size measurement based on electrical mobility, which is determined by scanning various size channels (Mostofi et al., 2012; Noël et al., 2018). Using a sampling port, we sampled the aerosolized EPFR particles inside the inhalation chamber with a tubing placed in the breathing zone of the animals, which was connected to the SMPS. Over a period of two days, during the 4-hour daily EPFR lo and hi exposures, we conducted either one 180 second scan every hour, or one 180 second scan every 15 minutes. This resulted in the collection of data from 4 scans on one day plus 20 scans on the other day, for a total of twenty-four 180 second scans for each EPFR lo and hi aerosol. The SMPS was operated with an aerosol flow rate of 0.5 L/min and a sheath flow rate of 2 L/min, allowing us to perform 180 second scans to determine particle size distribution with high resolution within a range of 17.2 to 982 nm. The CPC, which can count up to 10^7 particles/cm^3, was used to assess the particle number concentration in the aerosols. The SMPS spectrometer was operated according to the manufacturer's recommendation.

Dosimetry modelling for EPFRs aerosols

An *in-silico* Multiple-Path Particle Dosimetry (MPPD, Version 3.04) model was used to computationally estimate the deposition of EPFR particle burden in the mouse lung using our exposure paradigm. We used a computational dosimetry model of the B6C3F1 mouse strain scaled to the average weight of mice used in our study. Default breathing parameters (breathing frequency, tidal volume, functional residual capacity, upper respiratory tract volume, and inhalation/exhalation fractions) for the B6C3F1 mouse strain scaled to an appropriately sized mouse were considered during modeling. Particle characterization such as density of particles matrix, the median mobility diameter (measured with the SMPS), used as a proxy for the median aerodynamic diameter, geometric standard deviation (GSD), and the constant exposure paradigm for 4h/d for 5 d using whole-body exposure modeling was used for computational deposition modeling of EPFR hi and lo particles in the mouse lung compartment. The MPPD dosimetry model also considered the rate of particle clearance following pulmonary deposition.

Assessing pulmonary function

After 5 consecutive days of EPFR exposure, pulmonary function testing in mice was assessed the day of sacrifice using the *flexiVent* system (SCIREQ, Montreal, Canada), as previously described (Noël et al. 2022). In brief, mice (n = 7 – 8 per group) were first anesthetized using a ketamine/xylazine cocktail, then a tracheotomy was performed to insert a cannula into the trachea. Each mouse was connected to the *flexiVent* system to measure lung function *via* forced oscillation technique. We used the pre-defined script from the *flexiVent* system to measure respiratory system resistance (Rrs) using the single-

compartment model. We also challenged the mice with incremental doses of methacholine (0, 12.5, 25, 50 mg/mL) to determine a dose-response relationship. To ensure that the lung function measurements fit within a single-compartment model, only results with a coefficient of determination > 0.95 were accepted. For each mouse, Rrs was measured at least five times, and results were averaged. After collection of the lung function data, we euthanized the mice via an intraperitoneal injection of Beuthanasia-D.

Measures of vascular function assessed using wire myography.

After 5 consecutive days of EPFR exposure and immediately following the last inhalation exposure, the mice (n=13–16) were euthanized using 50 mg/kg pentobarbital injected intraperitoneally. Thoracic aortas were carefully dissected, cleaned of adventitia, cut into 3 mm rings, and placed in oxygenated, cold Krebs-Henseleit solution, pH 7.4. Arteries were analyzed in a random fashion. Vascular function was assessed as endothelium-dependent versus endothelium-independent vasorelaxation via wire myography (DMT, Ann Arbor, MI). Under a microscope, the artery rings were threaded carefully with thin titanium wire and were affixed to the jaws of a myograph, the chamber of which was filled with warm, oxygenated Krebs–Henseleit solution maintained at 37°C. Once secured, a resting tension of 9.8 mN was applied and the vessel was allowed to equilibrate. To maintain vessel viability, the Kreb's physiological salt solution was replaced every 15 min. After equilibration, phenylephrine (PE) was added at a concentration required to constrict the vessels to 80% of maximal contraction. Note that in advance of experimental measures, pilot studies were conducted on vessels from control animals to determine 1) the magnitude of resting tension required for optimal analyses, and 2) the concentration of PE required to achieve 80% maximal contraction. After the response to PE had reached a plateau, endothelium-dependent vasodilation was assessed by applying increasing concentrations of acetylcholine (ACh) to the chamber and assessing decreases in tension after each addition. The vessels were then washed thoroughly, re-equilibrated to 9.8 mN, and treated again with PE. After a plateau was reached, endothelium-independent vasorelaxation was assessed by applying increasing concentrations of sodium nitroprusside (SNP).

Plasma endothelin-1 and nitric oxide determination

Blood was collected in ethylenediamine tetra-acetic acid (EDTA)-coated polystyrene tubes. The plasma was immediately obtained by centrifuging at 2000 rpm for 10 min at 4°C. One half was stored at −80°C until analysis for levels of endothelin-1 (ET-1). Aliquots of the other half of the plasma sample were mixed 1:6 with potassium ferricyanide and *N*-ethylmaleimide in PBS+NP40 and kept at −80°C until analysis. Plasma ET-1 level was measured using a commercially available ELISA kit (Abcam, Cambridge, MA), according to the manufacturer's protocol. Any hemolyzed plasma was excluded from analysis. Plasma nitric oxide levels were determined by measuring the concentrations of nitrite, its stable metabolite, using a Sievers nitric oxide (NO) analyzer. Briefly, a 1% wt/vol solution of sodium iodide in acetic acid was used to generate a calibration curve ranging from 10 nM–10 μM. Samples were analyzed in a rotating order and a control was used in between each group to verify that no drift occurred between sample sets. The apparatus was cleaned, and fresh solutions were prepared frequently to ensure a rigorous analysis.

Gene Expression Analysis

Aortas and lungs were collected in cryovials with RNA-protect and were snap-frozen using liquid nitrogen. The samples were stored at −80°C until processed. The RNA was extracted from the samples using the RNeasy Mini Kit (Qiagen, Hilden, Germany). The concentration and purity were determined using a Nanodrop spectrophotometer. The quality of the isolated RNA was evaluated on an Agilent 5300 fragment analyzer system (Agilent Technologies, Santa Clara, CA). cDNA was prepared from the 1 μg RNA using iScript reverse transcription supermix (Bio-Rad, CA, USA) and diluted with RNase-free water. 25 ng cDNA was used to analyze the gene expression levels via Biorad CFX96 Touch real-time PCR machine (Biorad, CA, USA) using iTaqMan universal probe supermix (Biorad, CA, USA). The real-time PCR amplification settings were one cycle for polymerase activation and DNA denaturation at 95°C for 30 sec, 40 cycles of amplification step, which consists of denaturation at 95°C for 5 sec and annealing at 60°C for 30 sec. Hypoxanthine phosphoribosyl transferase (*Hprt*) was used as an internal reference gene to normalize the results. Gene expression was calculated using ΔΔCt method, and the fold change was calculated using the $2^{-\Delta\Delta Ct}$ method.

Flow Cytometry Analysis

After euthanasia, the lungs were removed from the mice (n = 8 per group). A flow cytometry method using an eleven-color panel was developed to identify specific lung cells expressing CYP1A1 in EPFR vs. filtered air-exposed mice. Lung cells were stained with live/dead viability dye, endothelial cells: CD31+, Leukocyte: CD45+, and epithelial cells: EpCAM+ along with the specific lung cells markers for progenitor basal cells: Krt5+, serous/club cells: CC10+, mucus cells: Muc5ac+, ciliated cells: α -tublin+, type II pneumocytes: Spc+, type I cells: T1a-biotin+.

For each mouse, both lungs were collected in a C-tube suitable for GentleMACS™ Octodissociator containing 2.4 ml of Hank's Balanced Salt solution (HBSS) on ice. Collagenase I (Invitrogen, NY) with a final concentration of 500 U/mL and DNase I (Sigma Aldrich, MO) with a final concentration of 2400 U/mL were added into each C-tube and coarsely pulverized in an Octodissociator. The pulverized lung was further incubated at 37° C in a shaker at 250 rpm for 20 min. Following incubation, the lungs were further subjected to dissociation with Octodissociator to reduce the remaining cell clumps and ensure a single cell suspension. Cells were strained through a 40 μm cell strainer. The resulting cell suspension was treated with RBC lysis buffer (eBioscience, San Diego, CA) to remove any residual blood cells. Further, the cells were stained with live/dead dye eFluor 780 (eBiosciences, San Diego, CA) and were subsequently fixed, permeabilized, and stained for inter and intracellular markers using antibodies PerCP-CD45 (eBiosciences, CA), PE-Cy7- CD31 (Biolegend, CA), APC-EpCAM (Biolegend, CA), and BV-421-Muc5ac (Novusbio, CO), BV785-T1a-biotin (Biolegend, CA), BV510- α -tubulin (Invitrogen, CA), PE-Dazzle-594-Spc+ (Bioss, MA), Alexa Fluor 647-Krt5 (Santa Cruz biotech), PE-CC10 (Santa Cruz biotech) and DyLight 488-CYP1A1 (Invitrogen, NY). A total of 1 million cells/ sample were analyzed by Cytek Aurora and dead cells were excluded from the analysis.

Statistical analysis

The experimental data are expressed as the means ± SEM unless otherwise indicated. Shapiro Wilk's and Levene's tests were used to determine the normality and equality of variance, respectively. For data that violated any of these assumptions, non-parametric Kruskal Wallis test was used. To determine significance between treatment groups that passed a test for normality and equality of variance, one-way analysis of variance (ANOVA) with Tukey's *post-hoc* tests were performed using Prism 9 for macOS (version 9.5.1) software (La Jolla, CA). In all cases, $p < 0.05$ was accepted as significant.

3. Results

Combustion-derived EPFRs have oxygen-centered free radicals and a long half-life.

Free radicals present in combustion-derived EPFRs were characterized using EPR. In brief, g-values derived from EPR spectra help to determine whether the radical is carbon- or oxygen-centered. The g-value for the EPFR hi and EPFR lo particles was 2.0028–2.0036, suggesting oxygen-centered free radicals. Both the g value and the peak shape were similar to spectra we obtained for PM derived from urban air (Dugas et al., 2016). The intensity of peaks detected in EPR correlates with the number of free radicals present. EPFR hi particles exhibited a higher intensity peak compared to EPFR lo, suggesting higher radical content for the EPFR hi particles. The half-life for the EPFR particles was ~ 208 days, suggesting the radicals were extremely stable. As indicated with a red dashed line (Figure 2B), the amount of free radical detected over time exhibited an exponential fit described by the equation $Y = 2.0E^{17}$ ê(-2E-^{04}) t, where Y is the EPFR concentration in spins/g and t is the aging time in hours.

Aerosolized EPFR particles collected from the exposure chamber were used for EPFR particle characterization. We observed similar aerosolized EPFR hi and EPFR lo particle sizes (Figure 3A) ranging from ~35 nm to 255 nm. EPFR hi and EPFR lo aerosolized particles were found to exhibit a 63.98 nm median mobility diameter with a 2.579 geometric standard deviation and a 98.33 nm median mobility diameter with 2.469 geometric standard deviation, respectively (Figure 3B & Supplemental Figure 2). However, TEM revealed that both EPFR hi and EPFR lo particle can form agglomerates reaching 0.1 to 0.2 μm in size (Supplemental Figure 3).

Dosimetry modeling shows EPFR hi and EPFR lo particles deposit in the lungs similarly to one another.

In silico multiple path particle dosimetry (MPPD) modeling was used to estimate the pulmonary deposition of EPFR hi and EPFR lo particles in mice after whole-body inhalation. The deposition fraction within the entirety of the respiratory tract or within a target region was estimated using the MPPD modeling software (version 3.04) by inputting parameters derived for EPFR hi and EPFR lo particle size distribution (including median mobility diameter (used as a proxy for the median aerodynamic diameter) and geometric standard deviation) and the density of the particles. MPPD modeling takes particle characterization into account in predicting the deposited dose of particles in each respiratory region and considers the particle's rate of clearance and retention. The predicted

deposition of EPFR particles in the differing respiratory compartments is shown in Figure 4A and 4B. Using dosimetry modeling, we observed similar deposition patterns for EPFR hi and EPFR lo aerosols in the upper respiratory tract (head), tracheobronchial (TB), and pulmonary (P) regions of the respiratory tract.

EPFR inhalation reduces lung function.

We performed *flexiVent* analysis to determine lung function following EPFR inhalation. Respiratory system resistance was measured using methacholine challenges in graded doses. Compared to filtered air-exposed animals, we found a significantly increased respiratory system resistance (Rrs) in EPFR hi-exposed mice challenged with 50 mg/mL methacholine (Figure 5). Increased respiratory resistance indicates an obstruction or narrowing of the airways, leading to a reduction in lung function.

EPFR exposure causes dose-dependent reduction in endothelial function.

Normal endothelial function is maintained by the physiologic balance of vasoconstricting agents like endothelin-1 (ET-1), and vasorelaxing agents like nitric oxide (NO). We measured plasma ET-1 and NO levels in mice exposed to filtered air, EPFR lo, or EPFR hi for 5 days. ET-1 levels were increased in a dose-dependent manner after EPFR exposures (30.6 pg/mL for filtered air controls vs. 40.8 pg/mL for EPFR lo and 44.6 pg/mL for EPFR hi, Figure 6A). Similarly, plasma NO levels were significantly reduced after EPFR exposure (236 nM for filtered air controls vs. 232 nM for EPFR lo vs. 137 nM for EPFR hi), again, in a dose-dependent manner (Figure 6B). Together with the significant increase in ET-1, these data suggest vascular endothelial dysfunction.

We next determined the functional response of the endothelium after exposure to EPFRs. Aortas were isolated from mice exposed to filtered air, EPFR lo, and EPFR hi for 5 d. Aortas from mice exposed to EPFRs exhibited a diminished acetylcholine (ACh)-induced vasodilation compared to filtered air treated animals. Specifically, we observed a significant reduction in vascular relaxation of aortas from EPFR hi exposed mice treated with ACh at the dose of 10^{-4}, 10^{-3} and 10^{-2} M ACh (Figure 7A). No significant difference in vasorelaxation was identified for treatment with sodium nitroprusside (SNP) (Figure 7B), an NO donor, suggesting that the observed impairment in vascular relaxation was endothelium dependent. These data, together with the plasma biomarkers of endothelial function support our hypothesis that the endothelium is an early target for EPFRs.

AhR- and antioxidant-responsive genes are increased after EPFR exposure.

AhR activation typified by environmental pollutants mediate a broad range of biological responses by modulating the expression of genes such as *Cyp1a1*, *Cyp1b1,* and *Aldh3a1* (Ma, 2008). AhR also regulates nuclear factor erythroid 2-related factor (NRF2) activation, leading to transcription of genes involved in antioxidant response signaling, including NAD(P)H quinone dehydrogenase 1 (*Nqo1)* and glutamate-cysteine ligase catalytic subunit (*Gclc*) (Ma, 2008; Zhong et al., 2013). Gene expression changes indicative of AhR activation and antioxidant response signaling were measured in the lungs and aorta of the mice exposed to EPFR for 5 days. We observed a significant increase in the antioxidant response gene *Nqo1* in the lungs of the mice exposed to EPFR hi compared to EPFR lo

and filtered air. Moreover, there was significant change in expression of *Gclc* in lungs when exposed to EPFR hi compared to EPFR lo (Figure 8B). However, *Nqo1* and *Gclc* were not significantly changed in the aorta (Figure 8B). In addition to changes in *Nqo1* and *Gclc*, we found a significant and robust increase in the expression of AhR responsive genes in the lungs and aorta after EPFR exposure (Figure 8A). The expression of *Cyp1a1* and *Cyp1b1* was significantly increased in the lungs of mice exposed to EPFR hi compared to EPFR lo and filtered air exposure. However, we identified similar significant increases in expression of *Cyp1a1* only in the aorta. Conversely, we observed a significant increase in *Aldh3a1* in lungs from mice exposed to EPFR hi compared to EPFR lo and filtered air, whereas it remained unchanged in aorta. Gene expression of AhR-activated responsive gene in the lungs and aorta suggested dose-dependent AhR activation by EPFRs and increased expression of antioxidant response genes in the lungs indicate pulmonary oxidative stress after EPFR inhalation.

EPFR exposure predominantly causes AhR activation in Alveolar Type -2 epithelial and club cells.

AhR activation leads to the transcription of the prototypical gene target *Cyp1a1*. Given our findings for increased expression of *Cyp1a1* in the lung, we sought to identify the cellular loci for AhR activation in the lung. We thus used flow cytometry to track CYP1A1 protein expression in individual, single cell suspensions of lung tissues derived from mice exposed to EPFR lo, EPFR hi and filtered air. The percentage of lung epithelial cells expressing CYP1A1 was significantly increased in mice exposed 5 days to EPFR hi compared to EPFR lo and filtered air (Figure 9A). Moreover, the percentage of epithelial cell-expressing CYP1A1 was predominantly identified to be alveolar type 2 cells (AT-2; 20%), but club cells (15%) also expressed CYP1A1 (shown in Figure 9B), indicating these two cell types were the predominant loci for increased AhR activation. There was negligible CYP1A1 expression in alveolar epithelial cells in EPFR lo and filtered air exposed mice (not shown). Together, these data suggest EPFR exposure promotes the dose-dependent activation of AhR in epithelial cells lining the alveoli and bronchioles.

4. Discussion

Epidemiological findings over the last twenty years have confirmed that PM exerts significant adverse impacts on human health, and the respiratory and cardiovascular systems are particular targets. Cardiopulmonary diseases, including heart disease, stroke, and lung cancer, have been linked to exposure to PM, and numerous studies have consistently shown a correlation between the concentration of airborne PM and the severity of cardiopulmonary events, indicating that increased levels of PM in air can lead to serious health consequences. Despite the known health risks of exposure, mechanisms underlying PM-induced health effects are still debated. Our laboratory and that of numerous others around the globe (Dela Cruz et al., 2014; Dellinger et al., 2000; Dellinger et al., 2001; Filippi et al., 2022; Gehling et al., 2014; Li et al., 2023; Lomnicki & Dellinger, 2003; Lomnicki et al., 2008; Runberg et al., 2020; Wang et al., 2019; Xu et al., 2021) are beginning to identify the health hazards of PM containing EPFR produced from a number of combustion sources (Al-Nu'airat et al., 2019; Hasan et al., 2020; Runberg et al., 2020; Xu et al., 2021; Zhao et al.,

2022). A major limitation of laboratory animal studies of PM-induced health effects is the inability to collect environmental PM in sufficient quantities for nose-only or whole-body inhalation studies. To facilitate mechanistic studies probing the health impacts of EPFRs in laboratory animals, we aimed to construct and characterize an exposure paradigm that enables EPFR-related toxicology studies in a typical laboratory setting. In studies presented here, we established a combustion method for producing EPFR-containing PM that closely mimics PM found in urban air. A particular novelty of these studies is that we were able to generate particles of consistent mass concentrations, but with differing concentrations of free radicals, thus enabling dose-response studies. With our newly developed TSCR system, we were able to generate EPFRs with a precise and controllable radical composition. Additionally, with the established reactor, we can control metal speciation and concentration in the EPFRs generated. This precise control over composition and chemical speciation enables our ability to elucidate the dose-dependent mechanism by which EPFRs impact cardiovascular and cardiopulmonary health. The characterization of EPFRs was reported in one of our earlier publications (P. Herring et al., 2013) documenting the combustion reaction of 1-methylnapthalene (1-MN) initiated by Fe(III) oxide nanoparticles. The same two stage combustion reactor (TSCR) is utilized in the current work for generation of EPFR hi or EPFR lo using slightly different initial content of fuel (e.g., anthracene 0.4% (w) and 1-monochlorophenol 13.6% (w)). In the earlier report (P. Herring et al., 2013), the low temperature matrix isolation-electron paramagnetic resonance (LTMI-EPR) (Khachatryan et al., 2006) was utilized to experimentally determine the superimposed signal of particulate from combustion of 1-MN. Using Brucker Symphonia software, the EPR spectrum of the particulate was simulated and found to be a mixture of organic carbon-centered radicals, oxygen-centered radicals, and soot. The carbon-centered radials were identified through simulation of the hyperfine structure to be 57.5% resonance-stabilized indenyl (Supplemental Figure 5A), 30% cyclopentadienyl (Supplemental Figure 5B) and 12.5% naphthalene 1-methylene radicals (Supplemental Figure 5C). Additionally, the oxygen-centered resonance-stabilized radicals (Supplemental Figure 5D) detected from the combustion reactor is consistent with the EPFR-based model in which organic radicals are stabilized by transition metal oxides (Dellinger et al., 2007; Truong et al., 2010; Vejerano et al., 2011). The EPR spectra of our generated EPFRs closely resembles the free radicals detected on the superfund thermal treatment sites (Cruz et al., 2012; Dela Cruz et al., 2014; Dela Cruz et al., 2011). The half-life of our generated EPFRs seems relatively stable over time, thus supporting their resemblance to the stable free radical derived from combustion sources (Cruz et al., 2012; Dela Cruz et al., 2014; Dela Cruz et al., 2011).

With our well-defined dry particle aerosolization, we were able aerosolize EPFR particles of similar mass concentrations but with varying radical concentrations. Moreover, there was no significant difference in particle sizes of EPFR hi and EPFR lo upon aerosolization. Thus, our whole-body exposure method achieved uniform particle size distribution of EPFRs particles during exposure within the chamber. Furthermore, computational dosimetry modeling showed that the EPFR hi and EPFR lo particles exhibit similar deposition patterns in lung compartments upon aerosolization, further strengthening our mechanistic study. The TSCR and dry particle aerosolization techniques developed in our study provide a basis

for the essential advancement needing for studying free radicals derived from combustion sources and their dose-dependent effects on cardiovascular and cardiopulmonary systems.

Our studies also highlighted that the laboratory generated PM method we developed here was successful in recapitulating the findings of epidemiology studies linking PM exposures with cardiopulmonary health effects. Specifically, our physiology-based studies demonstrated a significant impairment in both vascular and pulmonary function, with our vascular studies highlighting the endothelium as a particular target. Studies have shown that the endothelium plays an essential role in maintaining vascular function. Endothelial cells form the inner lining of blood vessels are necessary for maintaining barrier function and for controlling homeostasis by responding to systemic vasoactive factors, neurotransmitters, and hormones (Sandoo et al., 2010). The endothelium also plays a direct role in maintaining the vascular environment through its own production of vasoactive factors. Normal vascular homeostasis is maintained by balancing vasoconstrictive factors like endothelin-1 (ET-1), and vasodilatory agents, such as nitric oxide (NO) (Sandoo et al., 2010). In contrast, an imbalance between vasodilators and vasoconstrictors suggests endothelial dysfunction. We found that EPFRs cause an increase in endothelin-1 and a reduction in nitric oxide, suggesting endothelial dysfunction, an early event in the pathophysiology of many vascular diseases. We have also found that EPFRs lead to an impairment in endothelium-dependent vascular relaxation, indicated by a reduction in vasorelaxation induced by the endothelial-selective agonist acetylcholine. Furchgott and Zawadzki (Furchgott & Zawadzki, 1980) first demonstrated that vascular relaxation by acetylcholine requires the release of nitric oxide (NO) from the endothelial cells. NO is an endothelium-dependent vasodilator that plays a vital role in maintaining the basal vascular dilatory tone of blood vessels.

A potential limitation of this study is that we did not directly compare the impacts of EPFRs to non-EFPR containing particulates. However, we have previously performed studies with particles containing only organics (and lacking the metal oxide) and with particle substrates alone (Balakrishna et al., 2011; Harmon et al., 2018; Jaligama et al., 2018; Kelley et al., 2013; Lee et al., 2014; Thevenot et al., 2013; Wang et al., 2011). These studies (Balakrishna et al., 2011; Harmon et al., 2018; Jaligama et al., 2018; Kelley et al., 2013; Lee et al., 2014; Thevenot et al., 2013; Wang et al., 2011) demonstrate that the effects of EPFRs on living organisms are due to its function as a complex entity (i.e., organics without the metal oxide attached to particles and particles alone fail to induce the same extent of physiological/cellular/immunological effects of the EPFR). Furthermore, blocking either uptake of the EPFR or the oxidative stress induced by the EPFR abrogates their effects (Harmon et al., 2018; Jaligama et al., 2018; Lee et al., 2014; Thevenot et al., 2013; Wang et al., 2011). Additionally, our previous studies (Balakrishna et al., 2011; Harmon et al., 2018; Jaligama et al., 2018; Kelley et al., 2013; Lee et al., 2014; Wang et al., 2011) have shown that exposing animals to organics alone will have physiological effects since these organics by themselves are toxic; however, as stated above, with the EPFR particular, these organics are chemisorbed in a metal-organic complex and are not available for interaction outside of the complex under normal physiological conditions.

Oxidative stress drives the health impacts associated with environmental PM. Though transition metals are often linked with PM-dependent oxidative stress responses, the

mechanisms for PM-related health effects cannot be fully explained by its elemental composition alone (Daher et al., 2012; Kelly & Fussell, 2012; Oeder et al., 2012; Park et al., 2018). We propose the EPFRs are the missing links. Our previous findings demonstrated oxidative stress in the lungs upon exposure to EPFR (Harmon et al., 2021; Kelley et al., 2013). Studies have shown that in many toxicological exposures, the induction of cellular oxidative stress is mediated via AhR activation (Dalton et al., 2002; Jin et al., 2014; Reichard et al., 2005; Tsuji et al., 2011). We thus examined gene expression changes in the lungs and aorta, with a particular focus on genes that reflect the AhR and antioxidant response signaling pathways. In studies presented here, we found a significant increase in AhR-associated genes in the lungs after EPFR inhalation. The AhR is a ligand-activated transcription factor that mediates the toxic effect of many pollutants. Upon ligand activation, AhR forms a heterodimer with AhR nuclear translocator (ARNT), translocates to the nucleus, and binds to response elements to promote the transcription of genes such as *Cyp1a1*, *Cyp1b1, Aldh3a1* and other genes involved in cell cycle, migration and inflammation (Attafi et al., 2022; Bankoti et al., 2010; Marlowe & Puga, 2005; Strapáčová et al., 2018). Notably, throughout our studies, we have consistently found a significant increase in the lung gene expression of *Cyp1b1* following exposures to EPFRs-aerosols (Harmon et al., 2021; Figure 8A). Since *Cyp1b1* is a protein-coding gene also involved in the biotransformation of xenobiotics, this confirms that our *in vivo* EPFR exposure system was able to deliver the EPFR particles to the lungs of the mice, and this further indicates that the up-regulation of *Cyp1b1* may be a good biomarker of exposure to EPFRs. In addition, studies have established the connection between AhR-mediated pathways and the activation of NRF2-KEAP1 (Haarmann-Stemmann et al., 2012; Lawal, 2017). NRF2 is a transcription factor regulating the expression of antioxidant response element (ARE)-mediated genes and phase II enzymes (Itoh et al., 1999). It has been shown that activation (Beamer & Shepherd, 2013) of the AhR dissociates the NRF2-KEAP1 complex, leading to phosphorylation of NRF2 and its consequent migration into the nucleus and binding to the Maf protein (Haarmann-Stemmann et al., 2012; Kalthoff et al., 2010). This complex can bind to the ARE located in the promoter sequences of many genes, activating target genes such as *Nqo1, Gclc, Hmox1* and other antioxidant enzymes *etc*. We showed that EPFRs increase the pulmonary expression of *Cyp1a1*, *Cyp1b1*, and *Aldh3a1* (gene products suggesting AhR activation), as well as *Nqo1 and Gclc* (components of antioxidant response signaling *via* NRF2). *Gclc* and *Nqo1* genes are involved in the cellular defense against oxidative stress. *Gclc* encodes the regulatory subunit of glutamate-cysteine ligase, the rate-limiting enzyme for glutathione which is an essential antioxidant in cells (Lu, 2013), whereas *Nqo1* encodes NAD(P)H dehydrogenase, an enzyme that reduces quinones to hydroquinones, which plays a critical role in protecting the cellular membrane from peroxidative injury (Jaiswal, 2000). An increased expression in *Gclc* and *Nqo1* genes suggests and increased activation of protective mechanisms in response to induced oxidative stress pathways in the lungs. AhR activation pathways indirectly lead to the activation of genes involved in oxidative stress pathways via NRF2, thus initiating redox cycling and conferring further pulmonary toxicity.

The respiratory epithelium is the primary site for ultrafine (<100 nm) particle deposition and serves as a gatekeeper for the AhR (Schiering et al., 2017). We noted significantly increased AhR activation in the lung epithelial cells, mainly in the alveolar type-2 and club cells.

Alveolar epithelial cells are critical to gas exchange in the lungs and interact with capillary endothelial cells, forming an air-blood interface. About 90–95% of this area comprises Type 1 pneumocytes (AT-1s), with endothelial cells on their basolateral side (Filkelstein, 1990). However, Type 2 pneumocytes (AT-2s) flank both cell types and maintain homeostasis (Zscheppang et al., 2018). Upon exposure to toxicants, AT-1 cells are lost, but AT-2 cells differentiate into AT-1s to re-establish the air-blood barrier (Evans et al., 1975). Given their barrier-restoring function and their release of systemic mediators (Barkauskas et al., 2013; Mason, 2006), EPFR-induced AhR activation in AT2 cells may contribute to vascular dysfunction distal to the lung by releasing bioactive mediators into the blood. Moreover, we found that EPFR causes a dose-dependent increase in pulmonary resistance, suggesting reduction in lung function upon exposure.

5. Conclusions

In summary, these studies outlined and validated a method for the laboratory generation for combustion derived-EPFRs. We were able to produce EPFR-containing aerosols at consistent mass concentrations but with two different free radical concentrations that enabled our ability to establish a radical dose-response for pulmonary and vascular dysfunction. Our study also suggested a physiologic mechanism by which exposure to combustion-generated EPFRs induce an early disruption of vascular function, with the endothelium as its early prime target. Moreover, we showed that EPFRs reduce pulmonary function and dose-dependently increase genes associated with AhR and antioxidant response signaling. Finally, we have demonstrated how to modify our combustion-generated EPFR method to produce particles of varying organic and metal speciation to test whether sources of combustion-derived PM alter the mechanisms contributing to their health effects.

Supplementary Material

Refer to Web version on PubMed Central for supplementary material.

Acknowledgments

This work was supported by National Institute of Environmental Health Sciences Grants R21ES03006202 (T. R. Dugas) and P42ES013648 (T. R. Dugas and S. A. Cormier).

References cited:

Al-Nu'airat J, Dlugogorski BZ, Oluwoye I, Gao X, & Altarawneh M (2019). Effect of Fe2O3 nanoparticles on combustion of coal surrogate (Anisole): Enhanced ignition and formation of persistent free radicals. Proceedings of the Combustion Institute, 37(3), 3091–3099.

Alaghmand M, & Blough NV (2007). Source-dependent variation in hydroxyl radical production by airborne particulate matter. Environmental science & technology, 41(7), 2364–2370. [PubMed: 17438788]

Aryal A, Harmon AC, & Dugas TR (2021). Particulate matter air pollutants and cardiovascular disease: Strategies for intervention. Pharmacology & therapeutics, 223, 107890. [PubMed: 33992684]

Attafi IM, Bakheet SA, Ahmad SF, Belali OM, Alanazi FE, Aljarboa SA, Al-Alallah IA, & Korashy HM (2022). Lead Nitrate Induces Inflammation and Apoptosis in Rat Lungs Through the Activation

of NF-κB and AhR Signaling Pathways. Environmental science and pollution research, 29(43), 64959–64970. [PubMed: 35482242]

Balakrishna S, Saravia J, Thevenot P, Ahlert T, Lominiki S, Dellinger B, & Cormier SA (2011). Environmentally persistent free radicals induce airway hyperresponsiveness in neonatal rat lungs. Particle and fibre toxicology, 8(1), 1–13. [PubMed: 21235812]

Bankoti J, Rase B, Simones T, & Shepherd DM (2010). Functional and phenotypic effects of AhR activation in inflammatory dendritic cells. Toxicology and applied pharmacology, 246(1–2), 18–28. [PubMed: 20350561]

Barkauskas CE, Cronce MJ, Rackley CR, Bowie EJ, Keene DR, Stripp BR, Randell SH, Noble PW, & Hogan BL (2013). Type 2 alveolar cells are stem cells in adult lung. The Journal of clinical investigation, 123(7), 3025–3036. [PubMed: 23921127]

Beamer CA, & Shepherd DM (2013). Role of the aryl hydrocarbon receptor (AhR) in lung inflammation. Seminars in Immunopathology,

Çapraz Ö, & Deniz A (2021). Assessment of hospitalizations from asthma, chronic obstructive pulmonary disease and acute bronchitis in relation to air pollution in İstanbul, Turkey. Sustainable Cities and Society, 72, 103040.

Cesaroni G, Forastiere F, Stafoggia M, Andersen ZJ, Badaloni C, Beelen R, Caracciolo B, de Faire U, Erbel R, & Eriksen KT (2014). Long term exposure to ambient air pollution and incidence of acute coronary events: prospective cohort study and meta-analysis in 11 European cohorts from the ESCAPE Project. Bmj, 348.

Cohen AJ, Brauer M, Burnett R, Anderson HR, Frostad J, Estep K, Balakrishnan K, Brunekreef B, Dandona L, & Dandona R (2017). Estimates and 25-year trends of the global burden of disease attributable to ambient air pollution: an analysis of data from the Global Burden of Diseases Study 2015. The lancet, 389(10082), 1907–1918.

Cruz A. L. N. d., Cook RL, Lomnicki SM, & Dellinger B (2012). Effect of low temperature thermal treatment on soils contaminated with pentachlorophenol and environmentally persistent free radicals. Environmental science & technology, 46(11), 5971–5978. [PubMed: 22548284]

Daher N, Ruprecht A, Invernizzi G, De Marco C, Miller-Schulze J, Heo JB, Shafer MM, Shelton BR, Schauer JJ, & Sioutas C (2012). Characterization, sources and redox activity of fine and coarse particulate matter in Milan, Italy. Atmospheric Environment, 49, 130–141.

Dalton TP, Puga A, & Shertzer HG (2002). Induction of cellular oxidative stress by aryl hydrocarbon receptor activation. Chemico-biological interactions, 141(1–2), 77–95. [PubMed: 12213386]

Davis MW (2020). Waste Management in the United States. Environmental Issues Today: Choices and Challenges [2 volumes], 137.

Dela Cruz ALN, Cook RL, Dellinger B, Lomnicki SM, Donnelly KC, Kelley MA, & Cosgriff D (2014). Assessment of environmentally persistent free radicals in soils and sediments from three superfund sites. Environmental Science: Processes & Impacts, 16(1), 44–52. [PubMed: 24244947]

Dela Cruz ALN, Gehling W, Lomnicki S, Cook R, & Dellinger B (2011). Detection of environmentally persistent free radicals at a superfund wood treating site. Environmental science & technology, 45(15), 6356–6365. [PubMed: 21732664]

Dellinger B, Lomnicki S, Khachatryan L, Maskos Z, Hall RW, Adounkpe J, McFerrin C, & Truong H (2007). Formation and stabilization of persistent free radicals. Proceedings of the Combustion Institute, 31(1), 521–528. [PubMed: 25598747]

Dellinger B, Pryor WA, Cueto B, Squadrito GL, & Deutsch WA (2000). The role of combustion-generated radicals in the toxicity of PM2. 5. Proceedings of the Combustion Institute, 28(2), 2675–2681.

Dellinger B, Pryor WA, Cueto R, Squadrito GL, Hegde V, & Deutsch WA (2001). Role of free radicals in the toxicity of airborne fine particulate matter. Chemical research in toxicology, 14(10), 1371–1377. [PubMed: 11599928]

DiStefano E, Eiguren-Fernandez A, Delfino RJ, Sioutas C, Froines JR, & Cho AK (2009). Determination of metal-based hydroxyl radical generating capacity of ambient and diesel exhaust particles. Inhalation toxicology, 21(9), 731–738. [PubMed: 19242849]

Dugas TR, Lomnicki S, Cormier SA, Dellinger B, & Reams M (2016). Addressing emerging risks: scientific and regulatory challenges associated with environmentally persistent free

radicals. International journal of environmental research and public health, 13(6), 573. [PubMed: 27338429]

Eaton GR, Eaton SS, Barr DP, & Weber RT (2010). Quantitative Epr. Springer Science & Business Media.

Fang G, Gao J, Liu C, Dionysiou DD, Wang Y, & Zhou D (2014). Key role of persistent free radicals in hydrogen peroxide activation by biochar: implications to organic contaminant degradation. Environmental science & technology, 48(3), 1902–1910. [PubMed: 24422431]

Filippi A, Sheu R, Berkemeier T, Pöschl U, Tong H, & Gentner D (2022). Environmentally persistent free radicals in indoor particulate matter, dust, and on surfaces. Environmental Science: Atmospheres, 2(2), 128–136.

Furchgott RF, & Zawadzki JV (1980). The obligatory role of endothelial cells in the relaxation of arterial smooth muscle by acetylcholine. nature, 288(5789), 373–376. [PubMed: 6253831]

Gehling W, Khachatryan L, & Dellinger B (2014). Hydroxyl radical generation from environmentally persistent free radicals (EPFRs) in PM2. 5. Environmental science & technology, 48(8), 4266–4272. [PubMed: 24004313]

Haarmann-Stemmann T, Abel J, Fritsche E, & Krutmann J (2012). The AhR–Nrf2 pathway in keratinocytes: on the road to chemoprevention? Journal of Investigative Dermatology, 132(1), 7–9. [PubMed: 22158605]

Harmon AC, Hebert VY, Cormier SA, Subramanian B, Reed JR, Backes WL, & Dugas TR (2018). Particulate matter containing environmentally persistent free radicals induces AhR-dependent cytokine and reactive oxygen species production in human bronchial epithelial cells. PloS one, 13(10), e0205412. [PubMed: 30308017]

Harmon AC, Noël A, Subramanian B, Perveen Z, Jennings MH, Chen Y-F, Penn AL, Legendre K, Paulsen DB, & Varner KJ (2021). Inhalation of particulate matter containing free radicals leads to decreased vascular responsiveness associated with an altered pulmonary function. American Journal of Physiology-Heart and Circulatory Physiology, 321(4), H667–H683. [PubMed: 34415187]

Hasan F, Khachatryan L, & Lomnicki S (2020). Comparative studies of environmentally persistent free radicals on total particulate matter collected from electronic and tobacco cigarettes. Environmental science & technology, 54(9), 5710–5718. [PubMed: 32267684]

Herring MP, Khachatryan L, & Dellinger B (2015). Speciation of Iron (III) Oxide Nanoparticles and Other Paramagnetic Intermediates during High-Temperature Oxidative Pyrolysis of 1-Methylnaphthalene. World academy of science, engineering and technology, 9(7), 804. [PubMed: 26413257]

Herring MP, Potter PM, Wu H, Lomnicki S, & Dellinger B (2013). Fe2O3 nanoparticle mediated molecular growth and soot inception from the oxidative pyrolysis of 1-methylnaphthalene. Proceedings of the Combustion Institute, 34(1), 1749–1757. [PubMed: 25530732]

Herring P, Khachatryan L, Lomnicki S, & Dellinger B (2013). Paramagnetic centers in particulate formed from the oxidative pyrolysis of 1-methylnaphthalene in the presence of Fe (III) 2O3 nanoparticles. Combustion and flame, 160(12), 2996–3003. [PubMed: 25673882]

Itoh K, Ishii T, Wakabayashi N, & Yamamoto M (1999). Regulatory mechanisms of cellular response to oxidative stress. Free radical research, 31(4), 319–324. [PubMed: 10517536]

Jaiswal AK (2000). Regulation of genes encoding NAD (P) H: quinone oxidoreductases. Free Radical Biology and Medicine, 29(3–4), 254–262. [PubMed: 11035254]

Jaligama S, Patel VS, Wang P, Sallam A, Harding J, Kelley M, Mancuso SR, Dugas TR, & Cormier SA (2018). Radical containing combustion derived particulate matter enhance pulmonary Th17 inflammation via the aryl hydrocarbon receptor. Particle and fibre toxicology, 15, 1–15. [PubMed: 29298690]

Jin Y, Miao W, Lin X, Pan X, Ye Y, Xu M, & Fu Z (2014). Acute exposure to 3-methylcholanthrene induces hepatic oxidative stress via activation of the Nrf2/ARE signaling pathway in mice. Environmental toxicology, 29(12), 1399–1408. [PubMed: 23712962]

Kalthoff S, Ehmer U, Freiberg N, Manns MP, & Strassburg CP (2010). Interaction between oxidative stress sensor Nrf2 and xenobiotic-activated aryl hydrocarbon receptor in the regulation of the

human phase II detoxifying UDP-glucuronosyltransferase 1A10. Journal of Biological Chemistry, 285(9), 5993–6002. [PubMed: 20053997]

Kelley MA, Hebert VY, Thibeaux TM, Orchard MA, Hasan F, Cormier SA, Thevenot PT, Lomnicki SM, Varner KJ, & Dellinger B (2013). Model combustion-generated particulate matter containing persistent free radicals redox cycle to produce reactive oxygen species. Chemical research in toxicology, 26(12), 1862–1871. [PubMed: 24224526]

Kelly FJ, & Fussell JC (2012). Size, source and chemical composition as determinants of toxicity attributable to ambient particulate matter. Atmospheric Environment, 60, 504–526.

Khachatryan L, Adounkpe J, Maskos Z, & Dellinger B (2006). Formation of cyclopentadienyl radical from the gas-phase pyrolysis of hydroquinone, catechol, and phenol. Environmental Science & Technology, 40(16), 5071–5076. [PubMed: 16955909]

Lawal AO (2017). Air particulate matter induced oxidative stress and inflammation in cardiovascular disease and atherosclerosis: The role of Nrf2 and AhR-mediated pathways. Toxicology letters, 270, 88–95. [PubMed: 28189649]

Le GE, Breysse PN, McDermott A, Eftim SE, Geyh A, Berman JD, & Curriero FC (2014). Canadian forest fires and the effects of long-range transboundary air pollution on hospitalizations among the elderly. ISPRS international journal of geo-information, 3(2), 713–731. [PubMed: 36405525]

Lee GI, Saravia J, You D, Shrestha B, Jaligama S, Hebert VY, Dugas TR, & Cormier SA (2014). Exposure to combustion generated environmentally persistent free radicals enhances severity of influenza virus infection. Particle and fibre toxicology, 11(1), 1–10. [PubMed: 24382024]

Li H, Chen Q, Wang C, Wang R, Sha T, Yang X, & Ainur D (2023). Pollution characteristics of environmental persistent free radicals (EPFRs) and their contribution to oxidation potential in road dust in a large city in northwest China. Journal of Hazardous Materials, 442, 130087. [PubMed: 36206715]

Lingard J, Tomlin A, Clarke A, Healey K, Hay A, Wild C, & Routledge M (2005). A study of trace metal concentration of urban airborne particulate matter and its role in free radical activity as measured by plasmid strand break assay. Atmospheric Environment, 39(13), 2377–2384.

Lomnicki S, & Dellinger B (2003). A detailed mechanism of the surface-mediated formation of PCDD/F from the oxidation of 2-chlorophenol on a CuO/silica surface. The Journal of Physical Chemistry A, 107(22), 4387–4395.

Lomnicki S, Truong H, Vejerano E, & Dellinger B (2008). Copper oxide-based model of persistent free radical formation on combustion-derived particulate matter. Environmental science & technology, 42(13), 4982–4988. [PubMed: 18678037]

Lu SC (2013). Glutathione synthesis. Biochimica et Biophysica Acta (BBA)-General Subjects, 1830(5), 3143–3153. [PubMed: 22995213]

Ma Q (2008). Xenobiotic-activated receptors: from transcription to drug metabolism to disease. Chemical research in toxicology, 21(9), 1651–1671. [PubMed: 18707139]

Marlowe JL, & Puga A (2005). Aryl hydrocarbon receptor, cell cycle regulation, toxicity, and tumorigenesis. Journal of cellular biochemistry, 96(6), 1174–1184. [PubMed: 16211578]

Mary B, Petter L, Elissa W, Diane R, Joel D, Petros K, George R, George T, & Murray A (2013). Short-Term Exposure to Air Pollution and Lung Function in the Framingham Heart Study. ISEE Conference Abstracts,

Mason RJ (2006). Biology of alveolar type II cells. Respirology, 11, S12–S15. [PubMed: 16423262]

Morgan T, George A, Alvarez P, Millan M, Herod A, & Kandiyoti R (2008). Characterization of molecular mass ranges of two coal tar distillate fractions (creosote and anthracene oils) and aromatic standards by LD-MS, GC-MS, probe-MS and size-exclusion chromatography. Energy & Fuels, 22(5), 3275–3292.

Mostofi R, Noël A, Haghighat F, Bahloul A, Lara J, & Cloutier Y (2012). Impact of two particle measurement techniques on the determination of N95 class respirator filtration performance against ultrafine particles. Journal of Hazardous Materials, 217, 51–57. [PubMed: 22464753]

Motesaddi Zarandi S, Hadei M, Hashemi SS, Shahhosseini E, Hopke PK, Namvar Z, & Shahsavani A (2022). Effects of ambient air pollutants on hospital admissions and deaths for cardiovascular diseases: a time series analysis in Tehran. Environmental science and pollution research, 1–13.

Noël A, Charbonneau M, Cloutier Y, Tardif R, & Truchon G (2013). Rat pulmonary responses to inhaled nano-TiO 2: effect of primary particle size and agglomeration state. Particle and fibre toxicology, 10, 1–18. [PubMed: 23305071]

Noël A, Maghni K, Cloutier Y, Dion C, Wilkinson K, Hallé S, Tardif R, & Truchon G (2012). Effects of inhaled nano-TiO2 aerosols showing two distinct agglomeration states on rat lungs. Toxicology letters, 214(2), 109–119. [PubMed: 22944471]

Noël A, Verret CM, Hasan F, Lomnicki S, Morse J, Robichaud A, & Penn AL (2018). Generation of electronic cigarette aerosol by a third-generation machine-vaping device: application to toxicological studies. JoVE (Journal of Visualized Experiments)(138), e58095.

Noël A, Xiao R, Perveen Z, Zaman H, Le Donne V, & Penn A (2017). Sex-specific lung functional changes in adult mice exposed only to second-hand smoke in utero. Respiratory research, 18, 1–12. [PubMed: 28049526]

Oeder S, Dietrich S, Weichenmeier I, Schober W, Pusch G, Jörres R, Schierl R, Nowak D, Fromme H, & Behrendt H (2012). Toxicity and elemental composition of particulate matter from outdoor and indoor air of elementary schools in Munich, Germany. Indoor air, 22(2), 148–158. [PubMed: 21913995]

Oyana TJ, Lomnicki SM, Guo C, & Cormier SA (2017). A scalable field study protocol and rationale for passive ambient air sampling: a spatial phytosampling for leaf data collection. Environmental science & technology, 51(18), 10663–10673. [PubMed: 28805054]

Pan C-JG, Schmitz DA, Cho AK, Froines J, & Fukuto JM (2004). Inherent redox properties of diesel exhaust particles: catalysis of the generation of reactive oxygen species by biological reductants. toxicological sciences, 81(1), 225–232. [PubMed: 15201441]

Park M, Joo HS, Lee K, Jang M, Kim SD, Kim I, Borlaza LJS, Lim H, Shin H, & Chung KH (2018). Differential toxicities of fine particulate matters from various sources. Scientific reports, 8(1), 17007. [PubMed: 30451941]

Pope C 3rd (2000). Epidemiology of fine particulate air pollution and human health: biologic mechanisms and who's at risk? Environmental health perspectives, 108(suppl 4), 713–723. [PubMed: 10931790]

Pryor WA, Stone K, Zang L-Y, & Bermúdez E (1998). Fractionation of aqueous cigarette tar extracts: fractions that contain the tar radical cause DNA damage. Chemical research in toxicology, 11(5), 441–448. [PubMed: 9585474]

Rajagopalan S, Brauer M, Bhatnagar A, Bhatt DL, Brook JR, Huang W, Münzel T, Newby D, Siegel J, & Brook RD (2020). Personal-level protective actions against particulate matter air pollution exposure: a scientific statement from the American Heart Association. Circulation, 142(23), e411–e431. [PubMed: 33150789]

Reichard JF, Dalton TP, Shertzer HG, & Puga A (2005). Induction of oxidative stress responses by dioxin and other ligands of the aryl hydrocarbon receptor. Dose-Response, 3(3), dose-response. 003.003. 003.

Rice MB, Ljungman PL, Wilker EH, Gold DR, Schwartz JD, Koutrakis P, Washko GR, O'Connor GT, & Mittleman MA (2013). Short-term exposure to air pollution and lung function in the Framingham Heart Study. American journal of respiratory and critical care medicine, 188(11), 1351–1357. [PubMed: 24200465]

Runberg HL, Mitchell DG, Eaton SS, Eaton GR, & Majestic BJ (2020). Stability of environmentally persistent free radicals (EPFR) in atmospheric particulate matter and combustion particles. Atmospheric Environment, 240, 117809.

Sandoo A, Veldhuijzen van Zanten JJ, Metsios GS, Carroll D, & Kitas GD (2010). The endothelium and its role in regulating vascular tone. The open cardiovascular medicine journal, 4(1).

Schiering C, Wincent E, Metidji A, Iseppon A, Li Y, Potocnik AJ, Omenetti S, Henderson CJ, Wolf CR, & Nebert DW (2017). Feedback control of AHR signalling regulates intestinal immunity. nature, 542(7640), 242–245. [PubMed: 28146477]

Strapáčová S, Brenerová P, Krčmář P, Andersson P, van Ede KI, van Duursen MB, van den Berg M, Vondráček J, & Machala M (2018). Relative effective potencies of dioxin-like compounds in rodent and human lung cell models. Toxicology, 404, 33–41. [PubMed: 29738842]

Svatos RL (2022). Contaminated Sites. In Women in Infrastructure (pp. 361–389). Springer.

Thevenot PT, Saravia J, Jin N, Giaimo JD, Chustz RE, Mahne S, Kelley MA, Hebert VY, Dellinger B, & Dugas TR (2013). Radical-containing ultrafine particulate matter initiates epithelial-to-mesenchymal transitions in airway epithelial cells. American Journal of Respiratory Cell and Molecular Biology, 48(2), 188–197. [PubMed: 23087054]

Tian L, Koshland CP, Yano J, Yachandra VK, Yu IT, Lee S, & Lucas D (2009). Carbon-centered free radicals in particulate matter emissions from wood and coal combustion. Energy & Fuels, 23(5), 2523–2526. [PubMed: 19551161]

Truong H, Lomnicki S, & Dellinger B (2010). Potential for misidentification of environmentally persistent free radicals as molecular pollutants in particulate matter. Environmental Science & Technology, 44(6), 1933–1939. [PubMed: 20155937]

Tsuji G, Takahara M, Uchi H, Takeuchi S, Mitoma C, Moroi Y, & Furue M (2011). An environmental contaminant, benzo (a) pyrene, induces oxidative stress-mediated interleukin-8 production in human keratinocytes via the aryl hydrocarbon receptor signaling pathway. Journal of dermatological science, 62(1), 42–49. [PubMed: 21316925]

Valavanidis A, Fiotakis K, Bakeas E, & Vlahogianni T (2005). Electron paramagnetic resonance study of the generation of reactive oxygen species catalysed by transition metals and quinoid redox cycling by inhalable ambient particulate matter. Redox Report, 10(1), 37–51. [PubMed: 15829110]

Valavanidis A, Fiotakis K, Vlahogianni T, Papadimitriou V, & Pantikaki V (2006). Determination of selective quinones and quinoid radicals in airborne particulate matter and vehicular exhaust particles. Environmental Chemistry, 3(2), 118–123.

Valavanidis A, Iliopoulos N, Gotsis G, & Fiotakis K (2008). Persistent free radicals, heavy metals and PAHs generated in particulate soot emissions and residue ash from controlled combustion of common types of plastic. Journal of Hazardous Materials, 156(1–3), 277–284. [PubMed: 18249066]

Vejerano E, Lomnicki S, & Dellinger B (2011). Formation and stabilization of combustion-generated environmentally persistent free radicals on an Fe (III) 2O3/silica surface. Environmental Science & Technology, 45(2), 589–594. [PubMed: 21138295]

Walsh M, Cormier S, Varner K, & Dellinger B (2010). By-products of the thermal treatment of hazardous waste: Formation and health effects. EM (Pittsburgh, Pa.), 26.

Wang P, Thevenot P, Saravia J, Ahlert T, & Cormier SA (2011). Radical-containing particles activate dendritic cells and enhance Th17 inflammation in a mouse model of asthma. American journal of respiratory cell and molecular biology, 45(5), 977–983. [PubMed: 21493781]

Wang Y, Li S, Wang M, Sun H, Mu Z, Zhang L, Li Y, & Chen Q (2019). Source apportionment of environmentally persistent free radicals (EPFRs) in PM2. 5 over Xi'an, China. Science of the Total Environment, 689, 193–202. [PubMed: 31271986]

Woodward NC, Crow AL, Zhang Y, Epstein S, Hartiala J, Johnson R, Kocalis H, Saffari A, Sankaranarayanan I, & Akbari O (2019). Exposure to nanoscale particulate matter from gestation to adulthood impairs metabolic homeostasis in mice. Scientific reports, 9(1), 1–11. [PubMed: 30626917]

Wyatt LH, Weaver AM, Moyer J, Schwartz JD, Di Q, Diaz-Sanchez D, Cascio WE, & Ward-Caviness CK (2022). Short-term PM2. 5 exposure and early-readmission risk: A retrospective cohort study in North Carolina heart failure patients. American Heart Journal, 248, 130–138. [PubMed: 35263652]

Wyatt LH, Xi Y, Kshirsagar A, Di Q, Ward-Caviness C, Wade TJ, Cascio WE, & Rappold AG (2020). Association of short-term exposure to ambient PM2. 5 with hospital admissions and 30-day readmissions in end-stage renal disease patients: population-based retrospective cohort study. BMJ open, 10(12), e041177.

Xiao R, Perveen Z, Rouse RL, Le Donne V, Paulsen DB, Ambalavanan N, & Penn AL (2013). In utero exposure to second-hand smoke aggravates the response to ovalbumin in adult mice. American Journal of Respiratory Cell and Molecular Biology, 49(6), 1102–1109. [PubMed: 23898987]

Xie J, Teng J, Fan Y, Xie R, & Shen A (2019). The short-term effects of air pollutants on hospitalizations for respiratory disease in Hefei, China. International journal of biometeorology, 63, 315–326. [PubMed: 30680626]

Xu Y, Qin L, Liu G, Zheng M, Li D, & Yang L (2021). Assessment of personal exposure to environmentally persistent free radicals in airborne particulate matter. Journal of Hazardous Materials, 409, 125014. [PubMed: 33444952]

Yang H, Yan C, Li M, Zhao L, Long Z, Fan Y, Zhang Z, Chen R, Huang Y, & Lu C (2021). Short term effects of air pollutants on hospital admissions for respiratory diseases among children: A multi-city time-series study in China. International Journal of Hygiene and Environmental Health, 231, 113638. [PubMed: 33080524]

Zhang X, Gu W, Ma Z, Liu Y, Ru H, Zhou J, Zang Y, Xu Z, & Qian G (2020). Short-term exposure to ZnO/MCB persistent free radical particles causes mouse lung lesions via inflammatory reactions and apoptosis pathways. Environmental pollution, 261, 114039. [PubMed: 32220747]

Zhao J, Shen G, Shi L, Li H, Lang D, Zhang L, Pan B, & Tao S (2022). Real-world emission characteristics of environmentally persistent free radicals in PM2. 5 from residential solid fuel combustion. Environmental science & technology, 56(7), 3997–4004. [PubMed: 35262334]

Zhong Q, Mishra M, & Kowluru RA (2013). Transcription factor Nrf2-mediated antioxidant defense system in the development of diabetic retinopathy. Investigative ophthalmology & visual science, 54(6), 3941–3948. [PubMed: 23633659]

HIGHLIGHTS:

- A method for the generation of EPFRs that resemble those found in urban areas
- Particle aerosolization and whole-body inhalation technique for exposing rodents
- A comprehensive method for assessing the cardiopulmonary effects of EPFRs
- Identified the lung and vasculature as particular targets of EPFRs
- Suggests mechanisms mediating cardiopulmonary injury

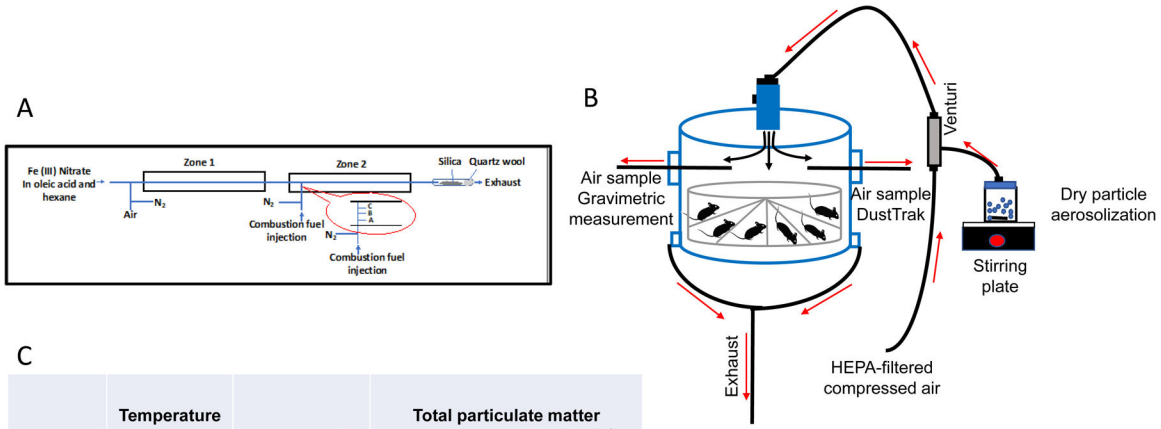

C

	Temperature (°C)	Humidity (%RH)	Total particulate matter concentration (TPM) (μg/m³)
Air	73.05±3.34	43.46±10.83	---
EPFR lo	73.99±1.64	44.68±9.10	278±49.9
EPFR hi	74.23±1.71	38.86±6.38	280±47.4

Figure 1:

A) Schematic view of the Two-Stage Combustion Reactor (TSCR) used to generate environmentally persistent free radicals (EPFRs) with controlled radical concentrations. The injection port temperatures were at (A) 400°C at 1 cm, (B) 700°C at 2 cm and (C) 940°C at 3 cm from the outside wall of the furnace and 975°C in the center of zone 2. B) Whole-body exposure set up showing the direction of air and particle flow into and out of the chamber. HEPA-filtered air was directed through the Venturi where the particles were aerosolized prior to being delivered into the 18 L plexiglass chamber. Aerosolized EPFRs were collected from the chamber for DustTrak, gravimetric measurements, transmission electron microscopy (TEM), and scanning mobility particle sizer (SMPS) during exposure. C) Tabular values of the average EPFRs exposure conditions inside the exposure chamber for 4 hours per day for 5 consecutive days.

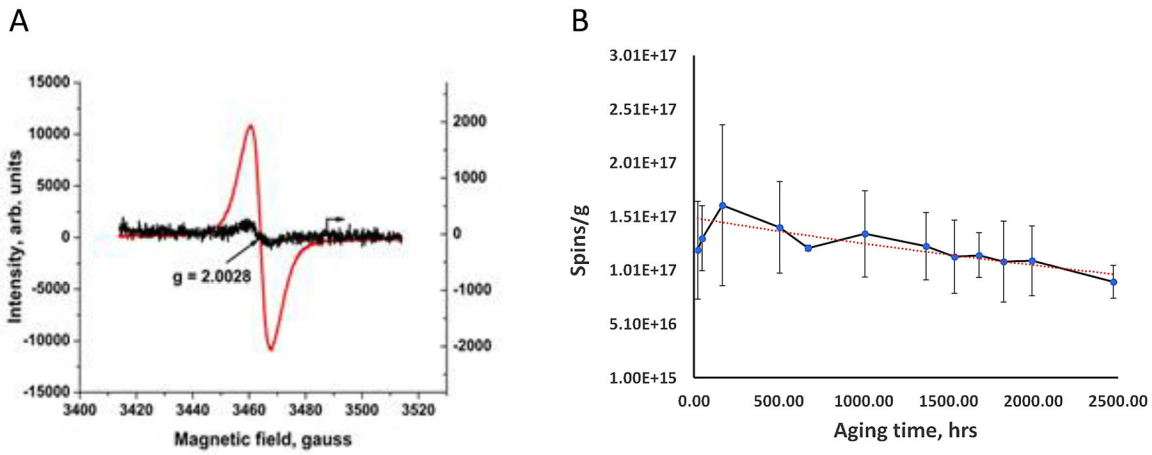

Figure 2:

A) EPR spectra obtained from EPFR hi and lo samples to determine the intensity of their radical signal (red curve represents EPFR hi and black curve represents EPFR lo). EPFRs display an asymmetrical g value (2.0028–2.0032) with a broad peak (ΔHp-p ~6 –10 Gauss). B) Rate of radical decay. Spins/g for an EPFR hi sample was plotted over time between June 30th and September 9th, 2020, and the rate of decay calculated to determine half-life of the radicals (red dashed line).

A

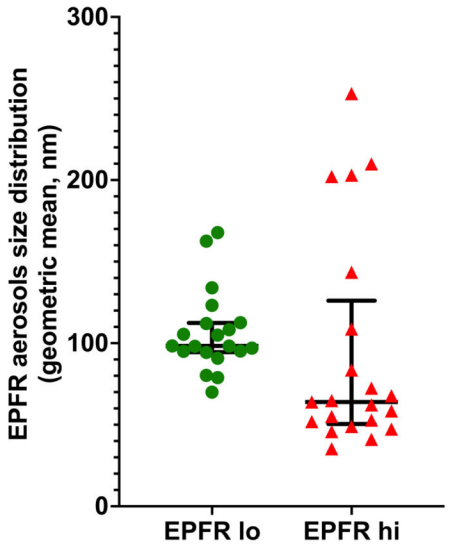

B

EPFR aerosols number concentration & size distribution		
	EPFR lo	EPFR hi
Number concentration (#/cm^3)	**2893**	**4556**
SD	1997	2460.0
Minimum (nm)	69.96	35.25
25% Percentile (nm)	94.56	50.43
Median (nm)	**98.33**	**63.98**
75% Percentile (nm)	112.5	126.1
Maximum (nm)	167.8	253
Mean (nm)	**106.4**	**93.88**
GSD	2.469	2.579

Figure 3:

A) The particulate size of aerosolized EPFRs was determined using a Scanning Mobility Particle Sizer (SMPS). There was no significant difference in aerosolized EFPR hi and EPFR lo particle size measured during exposure. B) Tabular form of EPFR aerosol numbers, concentration, and size distribution determined using SMPS during exposure.

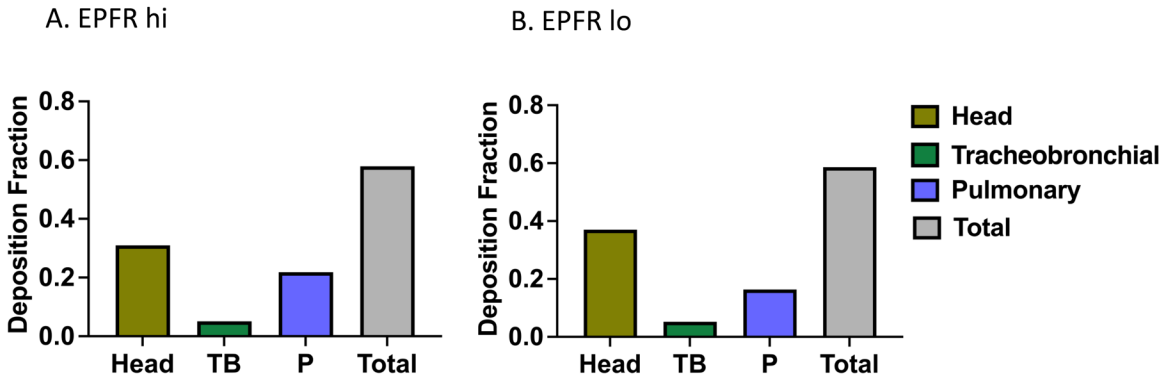

Figure 4:

MPPD modeling was used to estimate the respiratory tract deposition fraction for aerosolized EPFR particulates. EPFR hi (A) and lo (B) particle deposition in mouse respiratory tract was computationally determined using parameters derived from our aerosol characterization data and our exposure paradigm.

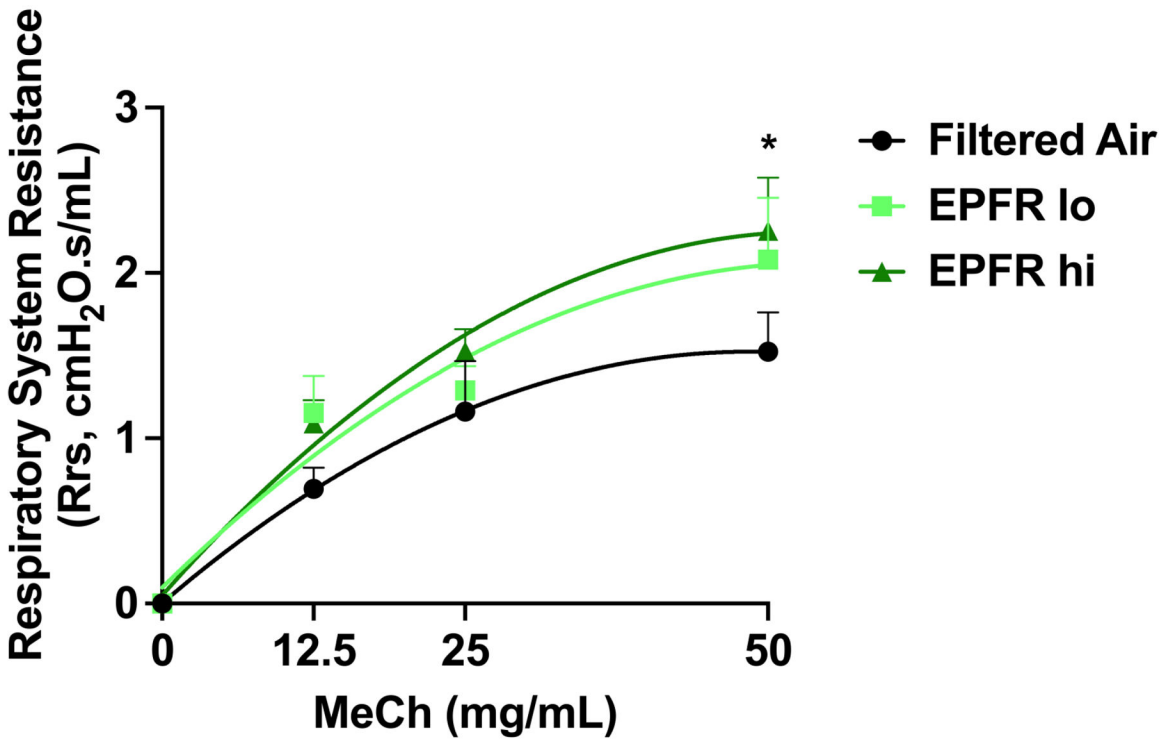

Figure 5:

Respiratory resistance as a measurement of lung function was determined *via flexiVent* using a forced oscillation technique. Mice exposed to filtered air, EPFR lo or EPFR hi (n=7–8/group) were assessed for respiratory resistance while administered increasing doses of methacholine so that a dose-response could be established. Mice exposed to EPFR hi experienced a significant increase in respiratory resistance compared to mice exposed to filtered air only. *Indicates $p<0.05$.

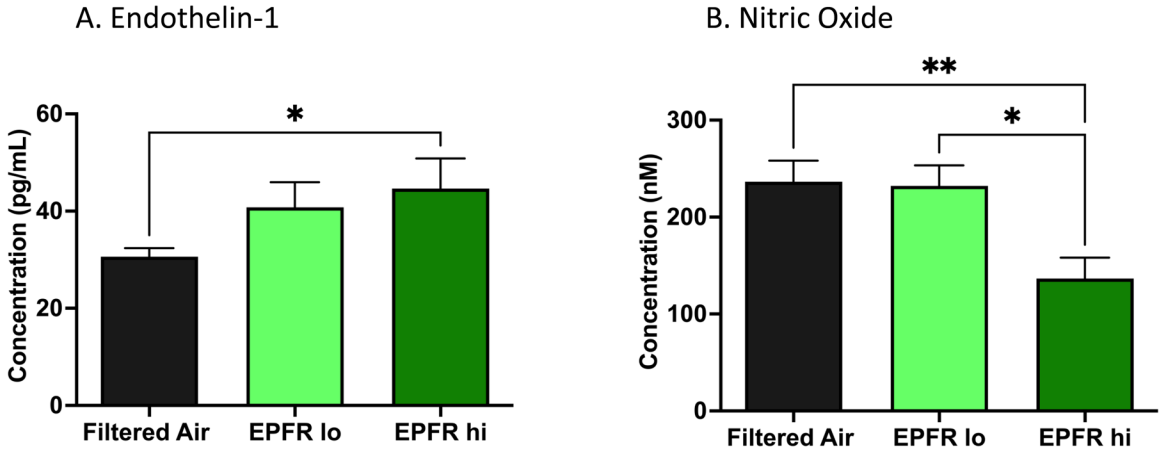

Figure 6:

Biomarkers of endothelial function were measured in the plasma of mice exposed to filtered air, EPFR lo and EPFR hi. A) The potent vasoconstrictive peptide endothelin-1 (ET-1) was increased in the plasma of mice exposed to EPFR hi versus filter air only. No change in plasma ET-1 levels was noted between mice exposed to EPFR lo versus filtered air (n=16–20/group. B) Nitric oxide (NO) was significantly reduced in the circulation of mice exposed to EPFR hi compared to EPFR lo and filtered air, while mice exposed to EPFR lo did not have significantly altered levels of NO (n=8–14/group). *Indicates $p<0.05$, **Indicates $p<0.01$.

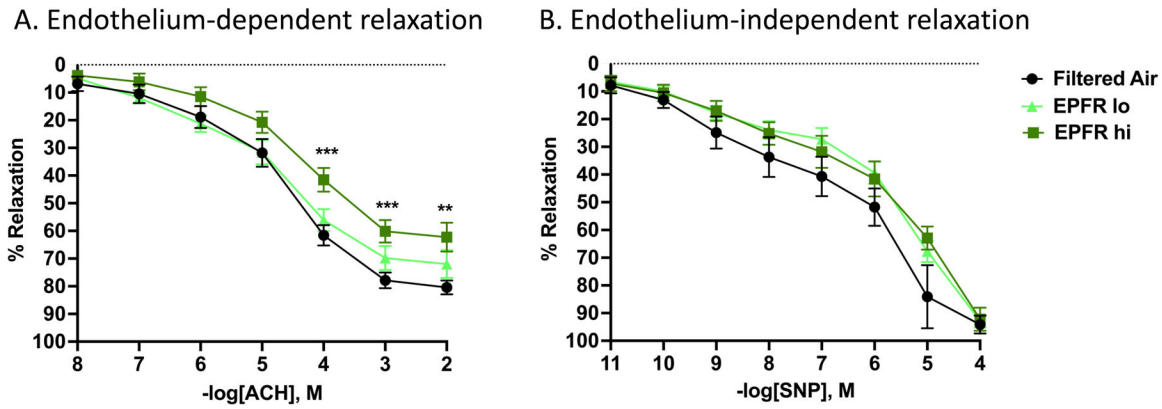

Figure 7:

Vessel reactivity was assessed for mice exposed to filtered air, EPFR lo or EPFR hi. A) Once vessels were constricted to 80% of their maximum contraction using phenylephrine (PE), increasing doses of acetylcholine (ACh) were administered to the bath and the resulting relaxation recorded. Mice exposed to EPFR hi, but not EPFR lo, demonstrated a significant impairment in relaxation at the highest three doses of ACh compared to mice exposed to filtered air only (n=13–16, $p<0.05$). B) Vascular responses to increasing doses of sodium nitroprusside (SNP) after constriction with PE were also assessed to confirm that the alterations in maximum relaxation were endothelium-dependent and not smooth muscle dependent. No significant changes in relaxation in response to SNP were noted between any of the three groups (n=13–16). **Indicates $p<0.01$, ***indicates $p<0.001$

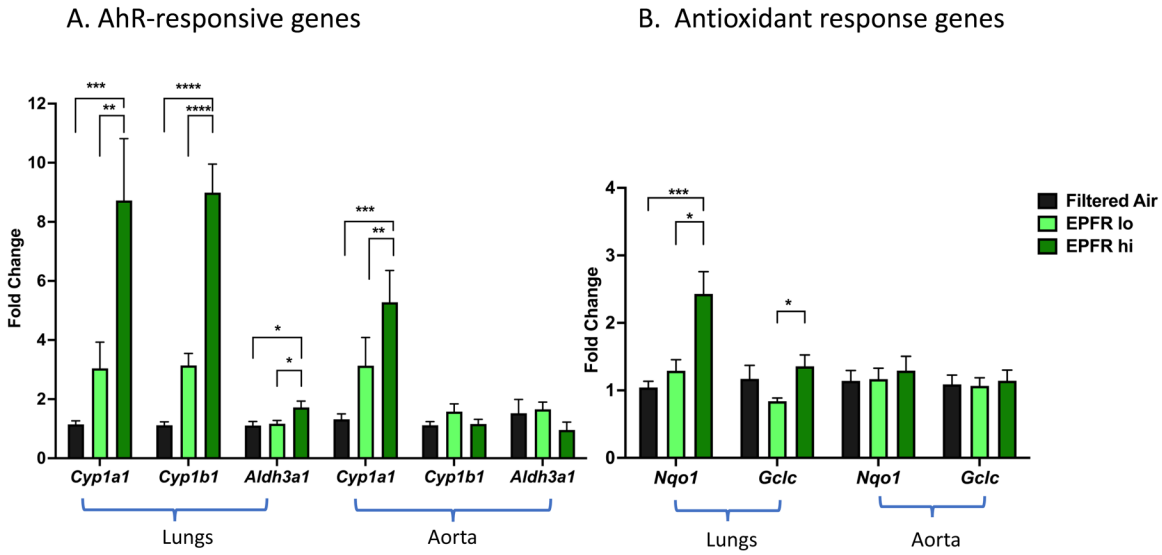

Figure 8:

Relative expression of A) AhR-responsive genes and B) antioxidant response genes measured in lungs and aorta of mice exposed to EPFR hi, EPFR lo and filtered air for 5 days (n=13–16) using real-time PCR. *Indicates $p<0.05$, **Indicates $p<0.01$, ***Indicates $p<0.001$, ****Indicates $p<0.0001$.

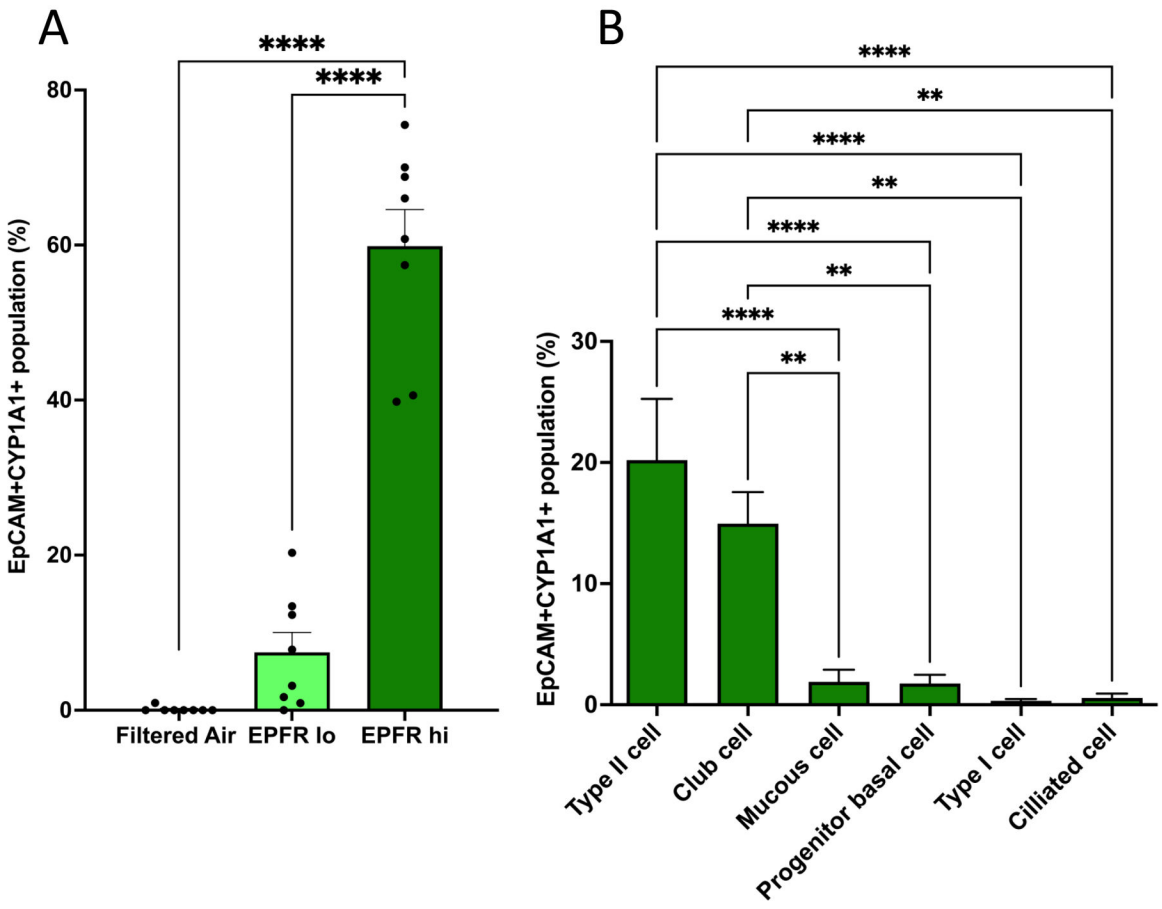

Figure 9:

Flow cytometry of lung epithelial cells using CYP1A1 expression as a marker for AhR activation. A) Analysis of epithelial cells identified a significant increase in CYP1A1 expression in lung cells from mice exposed to EPFR hi compared to lung cells from mice exposed to EPFR lo and filtered air (n=8/group, $p<0.05$). No increase in CYP1A1 expression was noted for EPFR lo exposed mice compared to filtered air exposed mice. B) Six different cell populations from the lungs of mice exposed to EPFR hi were assessed for CYP1A1 expression and reported as a percentage of each type of cell. Type II alveolar and club cells both expressed significantly more CYP1A1 than did the mucous, progenitor basal, type I alveolar or ciliated lung cells. CYP1A1 expression in six individual lung cell populations from mice exposed to filtered air and EPFR lo was negligible and is not shown. **Indicates $p<0.01$, ****Indicates $p<0.0001$